RuS_2 thin films as oxygen evolving electrocatalyst - highly oriented growth on single crystal FeS_2 substrates and on its properties compared to polycrystalline layers

Andreas Kratzig[1*], Carolin Zachäus, Stephan Brunken[1], Diana Thomas[2], Peter Bogdanoff[1], Klaus Ellmer[1], and Sebastian Fiechter[1*]

[1] Helmholtz-Zentrum Berlin für Materialien und Energie GmbH, Institute for Solar Fuels,
Hahn Meitner-Platz 1, D-14109 Berlin, Germany,

[2] MAX IV Laboratory, Lund University, SE-221 00 Lund, Sweden

Received

Dedicated to Prof. Wolfram Jaegermann on the occasion of his 60th birthday

PECS RuS_2, magnetron sputtering, electron microscopy, pol figures, phi-scans, remission spectroscopy, electrochemistry, oxygen evolution

* Corresponding authors: e-mail andreas.kratzig@helmholtz-berlin.de, fiechter@helmholtz-berlin.de,
Phone: +49-30-8062-42927,
Fax: +49-30-8062-42434

The compound semiconductor RuS_2, known as mineral laurite, has been investigated as a potential (photo)electrochemically active anode material for the oxygen evolution in the process of (photo)electrolytic water splitting. The contribution describes for the first time the preparation of RuS_2 thin films deposited on (100)- and (111)-oriented FeS_2 (pyrite) substrates using reactive magnetron sputtering. The epitaxial growth of 60 nm thick films was confirmed by X-ray diffractometry, texture measurements and the evaluation of cross section transmission electron micrographs. By optical reflectance spectroscopy and Seebeck coefficient measurements a direct band gap of 1.9 eV and p-type conductivity could be determined. Due to the modest electrochemical stability of the epitaxial layers in electrochemical investigations, polycrystalline films of laurite were also deposited on Ti sheets and Si wafers. As a function of grain size, [S]:[Ru] ratio and grain orientation highest activity towards oxygen evolution was found when the conditions were fulfilled that the layer composition was close to stoichiometry and increased particle sizes showed a strong textured in the grains. Some structural and chemical properties argue for the (100) surface as catalytically active and stable layer compared to other surfaces.

1 Introduction To convert sunlight into chemical energy in a photoelectrochemical cell, a device can be used which consists of at least one photoelectrode being able to split water under illumination with sunlight into oxygen and hydrogen [1]. The transition metal compound semiconductor RuS_2 with a direct band gap of $\leq$ 2.2 eV is in principle an appropriate material for this purpose [2]. Ezzaoui et al. were among the first studying light-assisted photooxidation of chloride and water using n-type RuS_2 single crystals [3-4]. Since laurite is a d-band semiconductor with a direct band gap at 2.2eV for the stoichiometric phase [2], a photovoltage in the range of 1.5 V should be achievable. However, even with RuS_2 single crystals only small photovoltages ($\leq$ 0.5 V) were measured due to bulk and surface states leading to a fast recombination of excited charge carriers [2-3]. Small single crystals showed an extraordinarily high stability towards electro-corrosion under oxygen evolving conditions [4]. Unfortunately, Ezzaouia et al. did not report which single crystal facet they exposed to the electrolyte [4]. Huang and Chen reported on a pronounced corrosion of their single crystal electrodes investigating (111) crystal faces as electrode surfaces [5]. Kühne, Jaegermann and Tributsch investigated the electrochemical stability of RuX_2 (X = S, Se, Te) single crystals before and after electrochemical oxygen evolution using X-ray photoelectron spectroscopy (XPS) [6]. They explained the high stability of the material against anodic corrosion by a high concentration of Ru 4d states at the valence band edge and a small overlap with sulfur p states compared to $RuSe_2$ and $RuTe_2$ which show distinguished corrosion phenomena under anodic polarization. From XP spectra they concluded on the formation of a ruthenium oxide covering the first monolayers on the exposed single crystal facet in contact with the electrolyte and a small amount of SO_x as corrosion product. The valence band spectrum of RuS_2 described by them was confirmed by Holzwarth et al., who experimentally determined the density of states of RuS_2 which were in agreement with their density functional theory calculations [7]. Studying the chemical and thermal stability of the laurite counterpart pyrite it could be verified that the most stable crystal facet were {100} faces [8] while especially faces of type {hkl} for $h,k,l \neq 0$ showed edge pits after the treatments.

For that reason, in this work the (photo)electrocatalytic behavior as a function of crystal orientation was studied growing epitaxial films of RuS_2 (laurite) on (100)- and (111)- oriented FeS_2 (pyrite) substrates. In addition, the electrochemical behavior of the grown epitaxial films was compared with polycrystalline, but textured laurite films.

2 Experimental

2.1 Substrate preparation Both, FeS_2 and RuS_2 crystallize in the cubic space group Pa$\bar{3}$ (point group $m/2\,\bar{3}$). Both compounds exhibit similar lattice constants, which allow an epitaxial growth of RuS_2 on FeS_2 (Table 1).

Table 1: Crystallographic parameters of FeS_2 and RuS_2

	FeS_2	RuS_2
Crystal system	cubic	cubic
Space group	Pa$\bar{3}$	Pa$\bar{3}$
Crystal class	$\boldsymbol{m/2\,\bar{3}}$	$\boldsymbol{m/2\,\bar{3}}$
Lattice constant a_0	5.41790 Å	5.61060 Å

Naturally occurring pyrite crystals from Murgul, Turkey, were used as substrates since FeS_2 single crystals can only be synthesized under very laborious and complicated conditions via chemical vapor transport (CVT). Hereby, only small single crystals of 4-5 mm edge length can be obtained [8-9]. Another motivation for the use of natural pyrite single crystals from Murgul is that they show a significant photoeffect upon illumination [10-12], which can support light-induced water splitting.

In order to prepare the substrates, the pyrite single crystals were oriented and fixed onto a holder with epoxy resin. Subsequently, the FeS_2 single crystals were cut into 1.5 mm thick wafers with a diamond wire saw. After removing the epoxy resin via ethyl acetate the pyrite wafers were cleaned with distilled water in an ultrasonic bath for 15 min. In a next step, the wafers were ground with sand paper of varying grain size and then evenly polished with diamond paste in several steps. The final polish was performed with a grain size of 0.1 µm, which created a reflective surface (see Fig. 1). After transfer into the evacuated sputter chamber the pyrite wafers were pre-treated for 30 min. at 300 °C under a defined H_2S atmosphere in order to remove the oxide layer from the surface. In addition, with this pre-treatment a gentle re-crystallization of the pyrite surface was achieved, which was before damaged by the process of polishing.

2.2 Film preparation and chemical composition

After a thermal pre-treatment of the pyrite substrate in H_2S atmosphere, laurite thin films were deposited by reactive magnetron sputtering using a metallic ruthenium target (diameter 4″, EVOCHEM, purity 99.9%) in a H_2S:Ar = 3:1 gas atmosphere. Sputtering was performed at a substrate temperature T_{sub} = 300 °C and at a sputtering pressure of p_{total} = 1.8 Pa. In order to guarantee a widely undisturbed epitaxial growth of RuS_2 on FeS_2 a sputter power of P ≤ 25 W in RF modus (radio frequency sputtering) was applied, which resulted in a deposition

rate of 0.5 nm/min. Typical film thicknesses were in the range from 55-60 nm and showed a homogeneous metallic brightness with a bluish-cyan lustre (Fig. 1).

In addition, polycrystalline films were deposited on Ti foils 0.1 mm thick varying the substrate temperature from RT to 600°C. The H_2S:Ar ratio in the gas phase was 3:1, the total pressure amounted to 2 Pa. RuS_2 layer thickness was ranging from 500 – 800 nm.

Selected laurite films were used to determine the [S] : [Ru] ratio by calibration-standard free Rutherford backscattering spectroscopy (RBS) using 1.7 MeV He^+ ions at a scattering angle of 170°. The spectra were evaluated by the simulation program RUMP [13] and the results used to calibrate energy dispersive X-ray fluorescence (EDX) data.

2.3 X-ray diffractometry and film texture analysis

All the films deposited were investigated by X-ray diffraction (XRD) in Bragg-Brentano geometry, using a Bruker AXS D8 Advance diffractometer. In order to achieve high resolution and a improved signal to noise ratio the X-ray beam was directed via a Göbel-mirror to the sample. To detect the diffracted radiation a SOL-X energy dispersive detector was employed. The measured diffractograms were analyzed with the software EVA3. In order to describe the crystallographic texture of the sputtered thin film pole figures were plotted based on equal-area stereographical projections [14]. The pole figures were performed on a laboratory 5-circle diffractometer (GE Inspection Technologies) using Cu-K_α as radiation source [15]. The parameters used were φ = [0°-360°] with $\Delta\varphi$ = 5°, ψ = [0°-85°] with $\Delta\psi$ = 5°, a measuring time of 10s per $\Delta\psi/\Delta\varphi$-setting and 2θ = 27.513° (position of the RuS_2 <111> diffraction peak) as well as 2θ = 31.875° (position of the RuS_2 <200> diffraction peak). Calculations of inverse pole figures were performed employing the software code “LaboTex” (Labosoft s.c.).

2.4 Transmission electron microscopy

Further structural investigations were carried out by using a high resolution transmission electron microscope (Philips CM12/ STEM), equipped with a system for energy dispersive X-ray fluorescence analysis (EDAX - Genesis) for the determination of the chemical composition. The measurements were performed at an acceleration voltage of 120 kV using a $LaBr_6$ cathode as electron source. The electron beam was focussed via a super TWIN lense, thereby a high resolution of 0.30 nm for point resolutions and 0.14 nm for line resolutions were achieved. Cross sections of the samples were prepared cutting the substrate with the RuS_2

film deposited on top into two halves, glueing them face-to-face and cutting with a diamond wire saw small bars of 0.5 mm thickness. The samples were subsequently sanded and polished to a thickness of 4-6 µm. In a last step ion milling (Baltec - RES 100) was used to prepare a grove the edges of which were analyzed by TEM.

2.5 Optical measurements – Kubelka Munk function

To determine the optical transitions of laurite including the fundamental band gap energy E_g, diffuse reflectivity (DR) was used. This method is a variation of the reflectance spectroscopy, which is applied primarily to polycrystalline materials or those having a very high absorption coefficient (~10^5/cm). The diffuse reflectance spectroscopy was carried out using the highly oriented RuS_2 thin films. The optical measurements were obtained in a double-beam spectrometer (Perkin Elmer Lamda 950 UV/Vis) using a halogen lamp (IR, VIS) and a deuterium lamp (UV) as radiation sources. The diffuse reflection of the sample was measured in the range from 300 to 1200 nm, using a scan rate of 30 nm/min and a scan increment 0.5 nm.
To better identify optical transitions, the measured reflection curves were converted using the representation by the Kubelka-Munk-function:

$$F(R_\infty) = \frac{(1+R_\infty)^2}{2R_\infty} = \frac{K}{S} \quad (1)$$

which is deduced from the ratio of absorption (K) and scattering coefficient (S) represented by a function of reflectivity (R) The detailed deviation of eq. (1) is described in refs. [16-17].
From the second derivative of the Kubelka-Munk function $d^2(F(R_\infty) \cdot E_{ph})^2/dE_{ph}$, the band gap of the laurite films assuming a direct optical transition was inferred.

2.6 Electrochemistry

Electrochemical measurements were carried out at room temperature in a three-electrode configuration using an electrochemical cell combined with a differentially pumped mass spectrometer [18-19]. The inlet system between the electrochemical cell and the differentially pumped vacuum system of the mass spectrometer (Balzers: QMI 420, QME 125, QMA 125 with an off-axis SEM) consists of a porous hydrophobic membrane, covered with a 100 nm thick Au-layer. This layer serves as a working electrode contact for the RuS_2 films which were attached to the gold layer. Oxygen produced by electrochemical experiments at the surface of the RuS_2 working electrode diffuses into the mass spectrometer where it is monitored simultaneously with the electrochemical data. The experiments were performed in N_2-purged

0.5M H_2SO_4 (pH 0) in a voltage range from 0.5 to 1.4 V/RHE at constant scan rates of 20 mV/s. As a reference, a mercury sulfate electrode (+680 mV/NHE) and as a counter electrode a Pt-wire were used. For the detection of photovoltage /-current, the samples were illuminated by a tungsten lamp of P = 40mW/cm².

3 Results and discussion

3.1 X-ray diffraction (XRD)

XRD measurements showed that the polished pyrite substrates exhibited the expected (111)- and (100)-orientation, respectively: studying (111)-oriented pyrite substrates, an intensive peak could be detected at 2θ = 28.512° (111) and a weaker one at 2θ = 59.012° (222) (Fig. 2.a, lower part). In the case of a (100)- oriented pyrite substrate, two characteristic peaks appear at 2θ = 33.040° (200) and at 2θ = 69.320° (400) (Fig. 2. (b), lower part). After deposition of a thin RuS_2 film, the coated pyrite substrates were measured again. Beside typical pyrite peaks, additional diffraction lines occur at slightly lower 2θ values, which are belonging to corresponding RuS_2 peaks (Figs. 2 (a) and 2 (b), upper part).

The RuS_2 peaks appear at lower 2θ angles because of the slightly larger lattice constant of the sulphide (see Table 1). The lattice mismatch between the two materials amounts to 3.5%.

Table 1: Miller indices (hkl) of FeS_2 (JCPDS # 01-071-2219) and RuS_2 peaks (JCPDS # 01-080-0669) with corresponding 2θ values [°]

hkl	FeS_2	RuS_2
111	28.512°	27.513°
222	59.012°	56.797°
200	33.040°	31.875°
400	69.320°	66.621°

Both sulphide phases show sharply defined peaks with high intensities, which points at a high degree of crystallinity of the substrate and of the thin RuS_2 film. However, from these measurements it cannot be decided whether the RuS_2 films were grown epitaxially or only with a preferred on the pyrite substrates. For that reason, texture measurements were performed, the results of which are presented as pole and inverse pole figures (see below).

3.2 Texture

From pole figures, propositions can be made about the crystallographic orientation of the crystalline grains in the film deposited on the pyrite substrate. Knowing the texture of the grown layers their structural properties can be related to its electrochemical properties. It was of interest to study the influence of lattice anisotropy of (100)- and (111)- oriented RuS_2 layers with respect to its (photo)electrochemical behaviour in the process of oxygen evolution (see Figures 3 (a) and 3 (b)).

RuS_2 thin layers sputtered on (100)- and (111)- oriented pyrite substrates show congruent pole figures, which underline the epitaxial growth of the laurite films on these substrates (see Figures 4-6). The uniform three- and fourfold symmetry of the pole figures representing the crystallographic orientation of the substrates and the thin layer grown on top supports this statement. By combination of data sets of pole figures of different reflections, it is possible to construct inverse pole figures from which statements on the crystallographic orientation / texture of the entire layer can be accomplished. Hereby, a uniform (111)- and (100)- orientation, respectively, of the sputtered laurite films (Fig. 6 (b)) as well as of the FeS_2 substrate (Fig. 6 (a)) could be verified. All parts of the (111)-oriented RuS_2 thin layer show the same crystallographic orientation in accord with the substrate. The same result has been obtained for the epitaxially grown RuS_2 thin film deposited on (100)-oriented FeS_2 substrates.

3.3 Transmission Electron Microscopy (TEM)

Figure 7 shows the cross section transmission electron micrograph of a RuS_2 thin layer, which is grown uniformly onto the substrate surface during the deposition process via reactive magnetron sputtering. In this figure a closed RuS_2 layer of a columnar structure is visible where the columns are grown perpendicular to the substrate surface. In the bulk of the substrate extended defects can be recognized as expected in a natural material. Although the RuS_2 films show all features of epitaxy evaluating XRD patterns and pole figures the layers are composed of columns which are epitaxially intergrown with the monocrystalline pyrite wafers. The columns of the RuS_2 layers are approximately 50 nm high and exhibit a diameter of about 10 nm (Fig. 6. (b)). In addition, the tops of the columns are facetted. An increased magnification (Fig. 6 (c)) however clearly indicates the epitaxial intergrowth of the RuS_2 columns with the FeS_2 substrate. The lattice planes of the substrate (FeS_2) perfectly continue from the bulk of the substrate into the lattice planes of a RuS_2 nano-column. By measuring distances of the lattice planes in a (100)- oriented film typical lattice plane distances of laurite (111 and 110) could be found.

3.4 Optoelectronic properties and chemical composition

To determine the conductivity type of the sputtered RuS_2 films the Seebeck coefficient was measured. Both, the (100)- as well as the (111)-oriented epitaxial films showed p-type conductivity, which can be explained by an excess of sulphur in the laurite lattice ([S]:[Ru] > 2:1). It is assumed that additional sulphur is not occupying interstitial lattice sites, but is caused by Ru vacancies in the pyrite lattice. The p-type conductivity can be explained under the assumption that these metal vacancies are charged. p-type conductivity of laurite films was also reported by Brunken *et al*. [20]. In this work, a [S]:[Ru] ratio of 2.1 was determined by RBS depositing polycrystalline layers of different thicknesses at a substrate temperature of 360°C, a H_2S : Ar ratio of 3:1, a DC power of 100 W and a total pressure ranging from 0.5 to 4.7 Pa. In the beginning of the layer formation an amorphous seed layer of about 20 nm thickness is formed. This result has been confirmed by additional experiments where we varied the deposition temperature from RT to 800°C.

Figure 7 (a) depicts $(F(R_\infty) \cdot E_{\mathrm{Ph}})^2$ as a function of the photon energy E_{Ph}. According to Kortüm [17] it is possible to infer the energetic position of optical transitions in the material calculating the second derivative $d^2(F(R_\infty) \cdot E_{ph})^2/dE_{ph}$ as a function of E_{ph}. The maxima in these curves represent the direct band gap which has a size of 1.9 eV for the (100)- and (111)- oriented laurite films (Fig. 7 (b)). Sulphur rich layers investigated by Brunken et al. and deposited at 360°C showed a direct band gap of 1.8 eV. Growing polycrystalline layers at increased substrate temperature the composition shifts towards an ideal [S] : [Ru] ratio of 2 (Fig. 8), which is correlated with an increase in band gap energy ≤ 2.1 eV (see ref. [2]). At temperatures higher than 460°C laurite becomes under the chosen sputter conditions unstable and decomposes into sulphur and ruthenium.

3.4 Electrochemical properties and structural features

Electrochemical measurements of the epitaxial RuS_2 thin films in the voltage range from 0.5 – 1,4 V/RHE led to a unexpected fast dissolution of the layers which is in contradiction to observations made before with single crystals [3-4,6]. The fact that the epitaxial layers are not closed, but composed of epitaxially aligned columns and pin holes confirmed by atomic force micrographs might be the reason for the observed fast dissolution. For that reason, the expected different behaviour of (100)- and (111)- oriented laurite interfaces in contact with an acidic electrolyte in the process of oxygen evolution could not be investigated. However

investigating polycrystalline films deposited on Ti substrates at different temperatures some tendencies of the electrochemical behaviour of the films related to the oxygen evolution reaction could be deviated. From Figs. 9 (a) – (c) it can be concluded that as a function of grain size, the [S]:[Ru] ratio and grain orientation highest activities towards the oxygen evolution reaction was found when the ratio in the layers was close to 2 and an increased particle sizes appeared showing a strong texture of the grains. SEM pictures (Fig. 10 (a) and (b)) show the morphology of the surfaces of two layers deposited at 240° and 460°C, which are characterized by a parallel intergrowth of cube-like individual particles which have a mean size of 10 to 30 nm, respectively. The high number of edges and corners of the smallest units visible show angles close to 90° what allows the conclusion that the (100) surfaces are the surfaces in contact with the electrolyte. Structurally they are distinguished by a mixed occupation of Ru and S atoms which are obviously electrochemically more stable than other surfaces (Fig. 9). With increasing size of the cubes at higher deposition temperatures the film composition approaches the ideal [S]:[Ru] ratio of 2 which is correlated with an improved catalytic behaviour towards oxygen evolution. This effect is correlated with a change of p- towards n-type conductivity. Further experiments are necessary to confirm this assumption.

In all cases no photoactivity could be observed. This fact can be explained by the still high number of point defects in the individual grains of the particles and the high number of grain boundaries in the epitaxial as well as in the polycrystalline films leading to a fast minority carrier trapping while majority carriers have a relatively long life time because of the trapping of minority carriers with a small cross section for majority carriers as shown by Time Resolved Microwave Conductivity [2]. It is assumed that the low mobility of the trapped minority charge carriers impede a migration to the surface and their participation at the expected light-assisted photoelectrochemical reaction in the oxidation of water.

4 Conclusions

We have demonstrated that (111)- and (100)- oriented RuS_2 thin films can be deposited by reactive magnetron sputtering on FeS_2 (pyrite) single crystal substrates of the correspondent orientation. Cross section transmission electron microscopy of the samples revealed that the layers are composed of epitaxially aligned columns of 50 to 60 nm height and ~10 nm thickness. The slightly p-type conductive films did not show any photoactivity as electrodes in the process of water oxidation (oxygen evolution) in an acidic electrolyte. In contrast to laurite single crystals and polycrystalline films, the thin layers corroded after a short time during the

cyclic voltammetry. Polycrystalline layers deposited at different temperatures show a significant dependency as electrocatalysts as a function of particles size, particle morphology and [S]:[Ru] ratio in the films. Films of nearly stoichiometric composition are characterized by small Seebeck coefficients and a direct band gap of ~2.2 eV.

References

1 S. Fiechter, in: Hydrogen Science and Engineering, edited by D. Stolten (WILEY-VCH, Darmstadt, 2014) 17 p.

2 P. Bogdanoff, C. Zachäus, S. Brunken, A. Kratzig, K. Ellmer, and S. Fiechter, Phys. Chem. Chem. Phys., **15**, 1452 (2013).

3 H. Ezzouia, R. Heindl, R. Parsons, and H. Tributsch, *J. Electroanal. Chem*. **165**, 155 (1984).

4 H. Ezzouia, R. Heindl, R. Parsons, and H. Tributsch, *J. Electroanal. Chem*. **145**, 279 (1983).

5 Y.-S. Huang and Y.-F. Chen, Phys. Rev. B **38**, 7997 (1988).

6 H.-M. Kühne, W. Jaegermann, and H. Tributsch, *Chem. Phys. Letters.* **112**, 160 (1984).

7 N. A. W. Holzwarth, S. Harris, and K. S. Liang, *Phys. Rev. B* **32**, 3745 (1985).

8 N. Alonso-Vante, G. Chatzitheodorou, S. Fiechter, N. Mgoduka, I. Poulios, and H. Tributsch, Solar Energy Materials **18**, 9 (1988).

9 S. Fiechter, J. Mai, A. Ennaoui, and W. Szacki, J. Crystal Growth **78**, 438 (1986).

10 A. Ennaoui, S. Fiechter, W. Jaegermann, H. Tributsch, J. Electrochem. Soc **133**, 97 (1986).

11 R. Schieck, A. Hartmann, S. Fiechter, H. Wetzel, and R. Könenkamp, J. Mater. Res. **5**, 1567 (1990).

12 A. Ennaoui, S. Fiechter, C. Pettenkofer, N. Alonso.-Vante, K. Büker, M. Bronold, C. Höpfner, and H. Tributsch, Solar Energy Materials and Solar Cells **29**, 289 (1993).

13 L.R. Doolittle, Nucl. Instrum. Methods Phys. Rev. B **9,** 344 (1985) and **15,** 227 (1986).

14 U. F. Kocks, C. N. Tomé, and H.-R. Wenk, Texture and Anisotropy, Cambridge University Press, Cambridge, United Kingdom (1998)

15 C. Genzel, Advances in X-ray Analysis, **44**, 247 (2001).

16 W. M. Wendlandt, H.G. Hecht, Reflectance Spectroscopy, InterscicencePublishers, John Wiley, New York, 1966.

17 G. Kortüm, Reflexionsspektroskopie, Springer, Berlin, 1969.

18 P. Bogdanoff, and N. Alonso-Vante, Ber. Bunsenges. Phys. Chem. **97**, 940 (1993).

19 P. Bogdanoff, and N. Alonso-Vante, J. Electroanal. Chem. **379**, 415 (1994).

20 S. Brunken, A. Kratzig, P. Bogdanoff, S. Fiechter, and K. Ellmer, Thin Solid Films, **527**, 16 (2013).

Figures

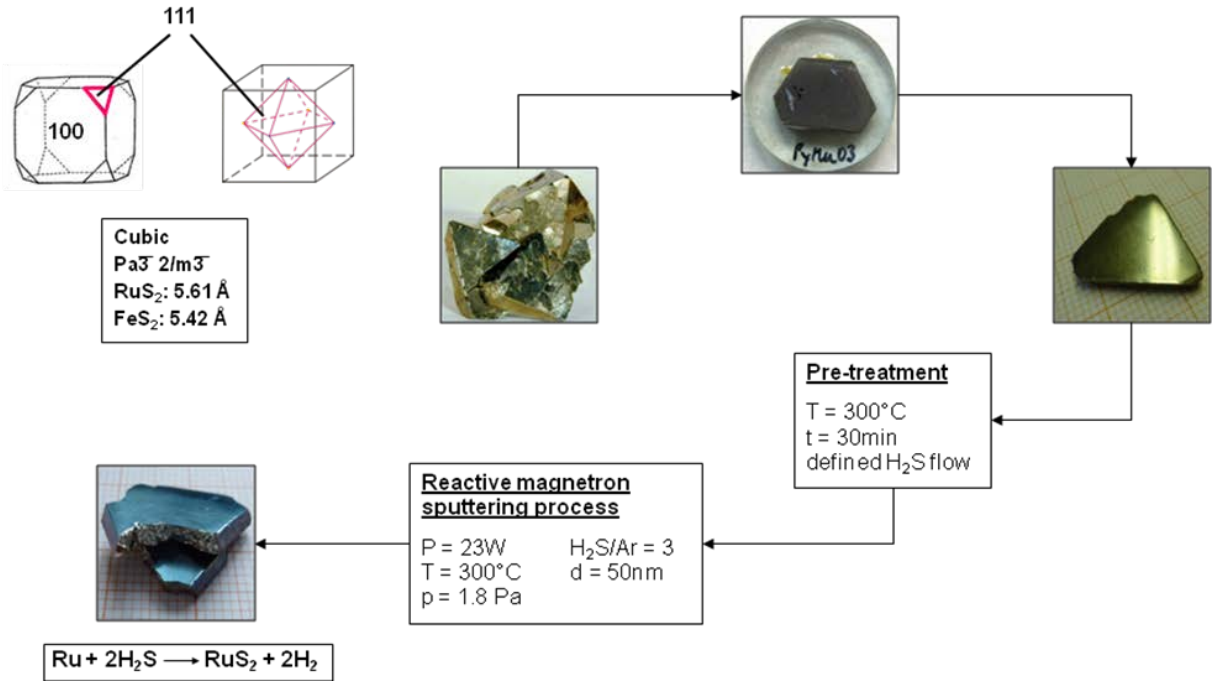

Fig. 1 Flow diagram displaying the preparation of oriented pyrite substrates and the subsequent RuS_2 film deposition using reactive magnetron sputtering.

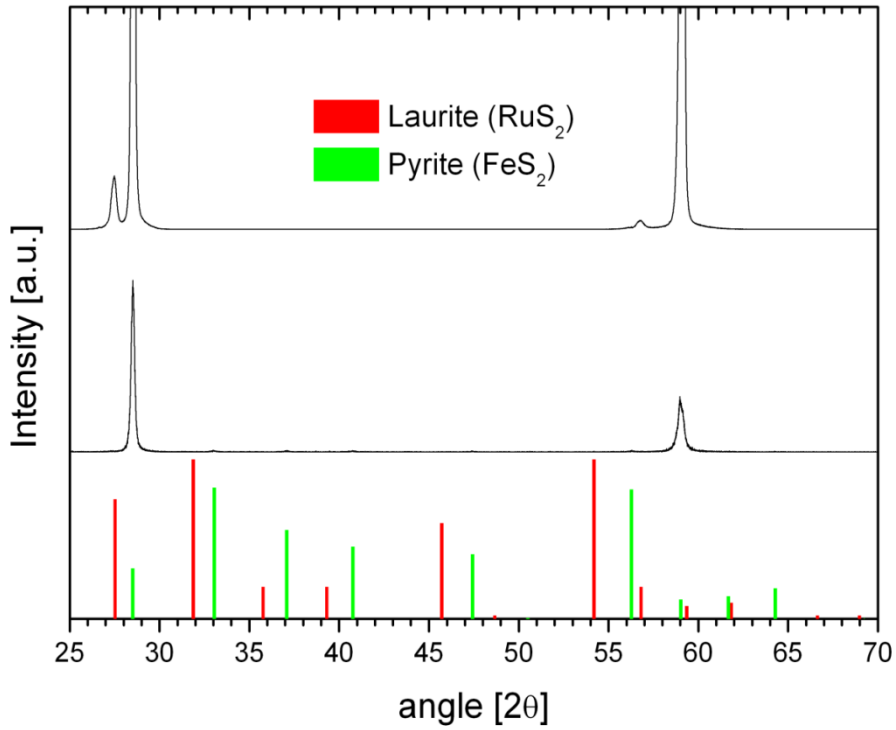

Fig. 2 (a) X-ray diffractograms of a (111)-oriented pyrite substrate (bottom) and of the same substrate after deposition of a 60 nm thick laurite layer (top). For reasons of comparison also the bar charts of the diffraction patterns of pyrite and laurite are given.

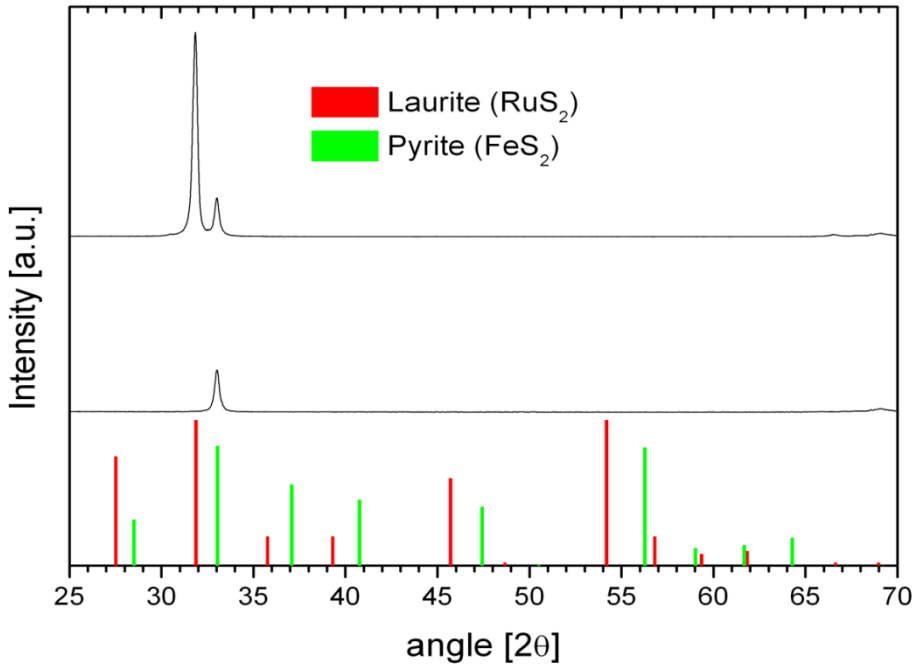

Fig. 2 (b) X-ray diffractograms of a (100)-oriented pyrite substrate (bottom) and of the same substrate after deposition of a 60 nm thick laurite layer (top). For reasons of comparison also the bar charts of the diffraction patterns of pyrite and laurite are given.

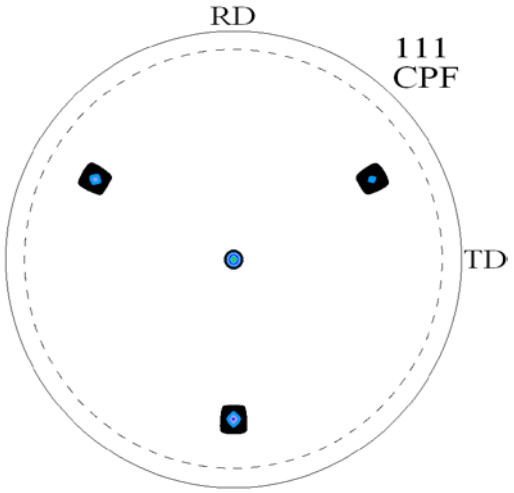

Fig. 3 (a) Pole figure of a (111)-oriented thin film of RuS_2 using Cu-K_α as radiation source. The measurement was performed at an angle of $2\theta = 27.513°$, which belongs to the RuS_2 <111> peak position.

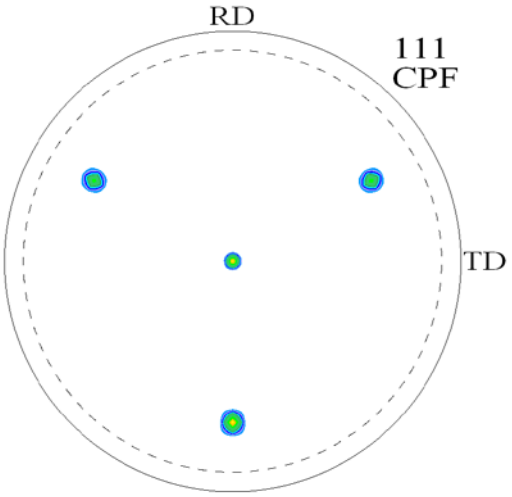

Fig. 3 (b) Pole figure of a (111)-oriented pyrite crystal substrate using Cu-K_α as radiation source. The measurement was performed at an angle of $2\theta = 28.512°$ which belongs to the FeS_2 <111> peak position.

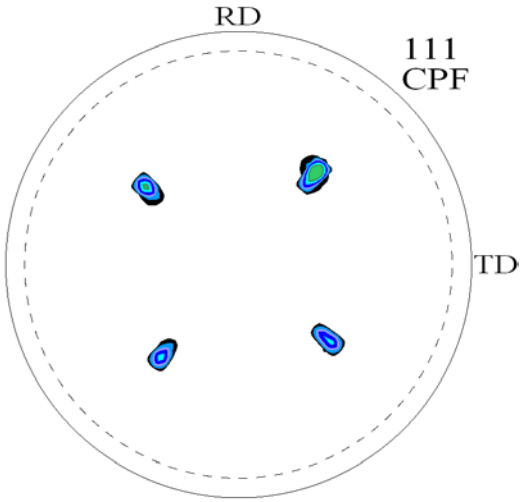

Fig. 4 (a) Pole figure of a (100)-oriented thin film of RuS_2 using Cu-K_α as radiation source. The measurement was performed at an angle of $2\theta = 31.875°$, which belongs to the RuS_2 <200> peak position.

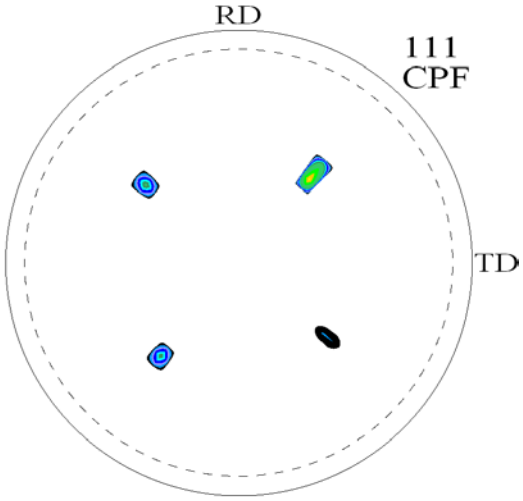

Fig. 4 (b) Pole figure of a (100)-oriented pyrite crystal substrate using Cu-K_α as radiation source. The measurement was performed at an angle of $2\theta = 33.040°$ which belongs to the FeS_2 <200> peak position.

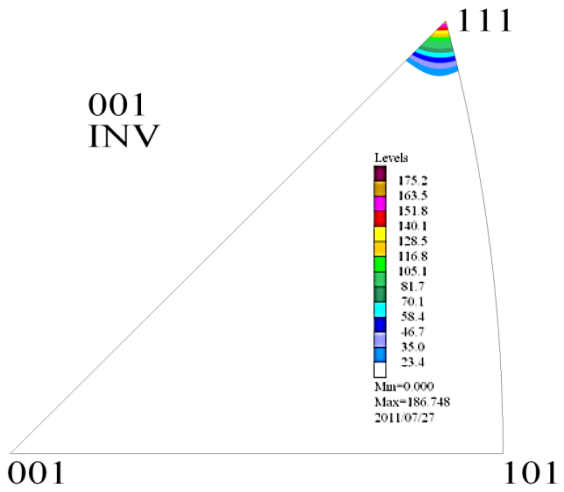

Fig. 5 (a) Inverse pole figure of an (111)-oriented substrate of pyrite proofing the high degree crystal orientation.

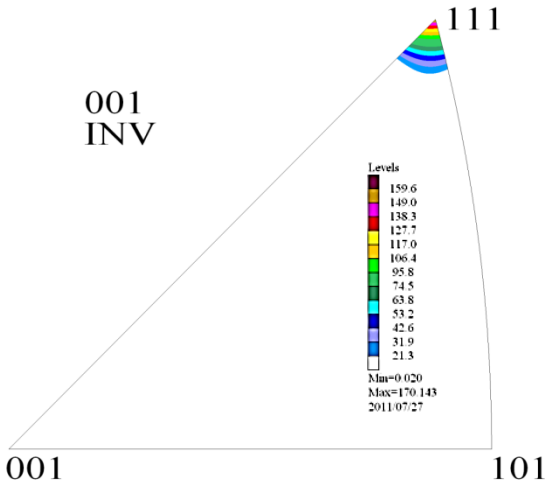

Fig. 5 (b) Inverse pole figure of a thin film of laurite film deposited on a (111)-oriented pyrite substrate.

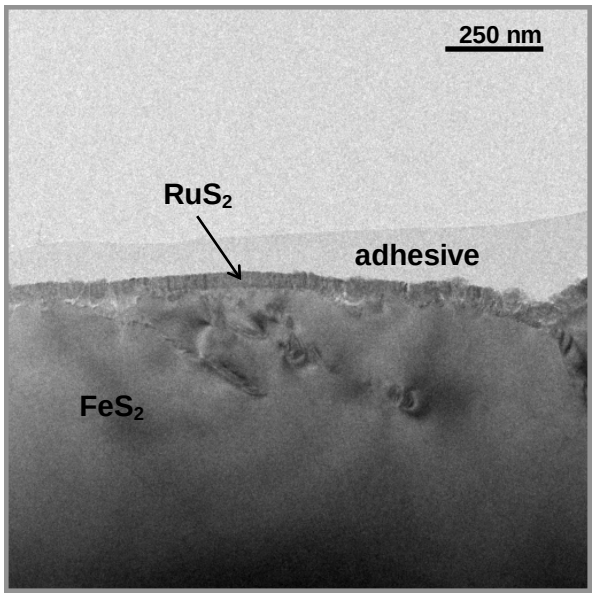

Fig. 6 (a) TEM cross section picture of a RuS_2 thin film of ~60 nm thickness, deposited on a pyrite substrate.

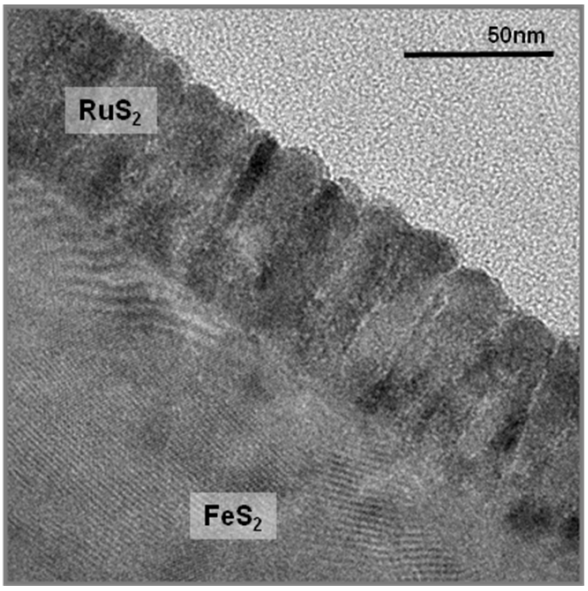

Fig. 6 (b) TEM cross section picture of a columnar grown RuS_2 film deposited on a single crystal pyrite substrate.

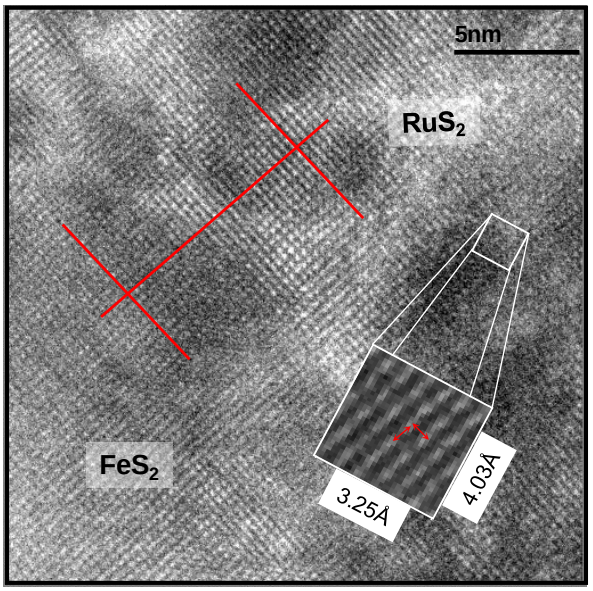

Fig. 6 (c) TEM cross section picture of a RuS_2 film deposited on (111)- oriented pyrite single crystal substrate. Shown is the epitaxial growth of a laurite column on the pyrite substrate close to the interface. The measured value of 3.25 Å is in accord with the (111) lattice plane distance, the value of 4.03 Å is close to the (110) lattice plane distance.

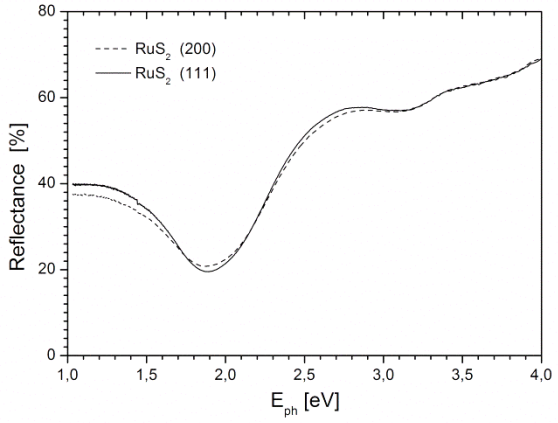

Fig. 7 (a) Square of the Kubelka Munk function times E_{ph} $(F(R_\infty) \cdot E_{ph})^2$ as a function of E_{ph} deviated from a remission spectra of sputtered RuS_2 films deposited on a FeS_2 single crystal wafer.

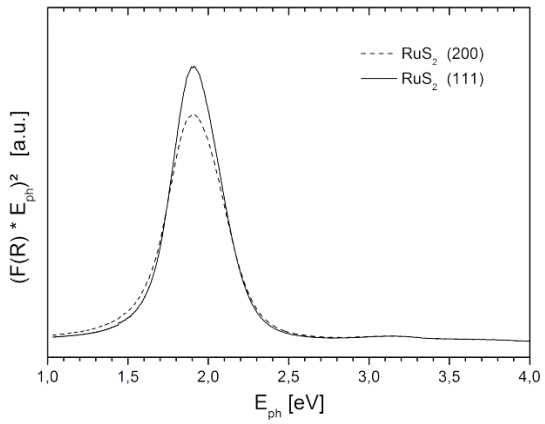

Fig. 7 (b) Second derivative of $(F(R_\infty) \cdot E_{ph})^2$ as a function of E_{ph}. The peak position represents the direct band gap of the RuS_2 thin film deposited on a FeS_2 substrate.

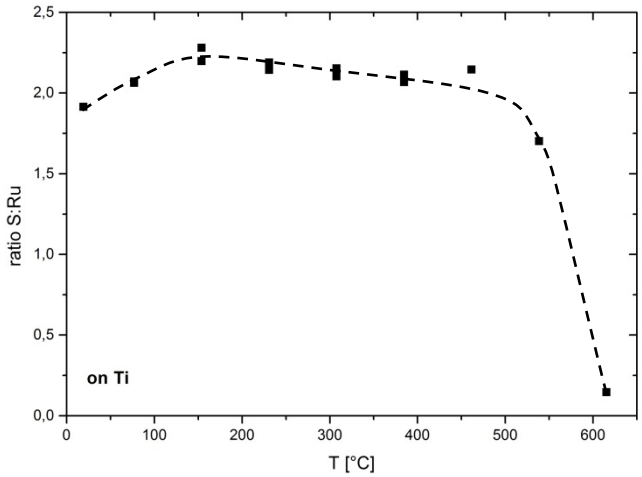

Fig. 8 (a) [S]:[Ru] ratio of laurite layers deposited on Ti substrates. The values were obtained from RBS and EDX measurements. With increasing temperature the composition is approaching the stoichiometric value of 2 while at temperatures above 460°C laurite continuously decomposes into volatile sulfur species and metallic Ru.

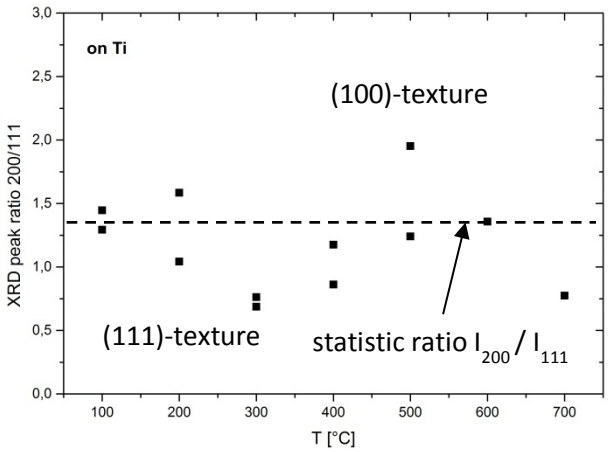

Fig. 8 (b) Intensity ratio of <200>vs.<111> XRD peaks of sputtered laurite films deposited at different temperatures. While a (111) texture is pronounced at 300°C statistically oriented or even (100)-textured films are favored growing layers at temperatures up to 460°C. At temperatures above 460°C laurite is no longer stable under the chosen H_2S pressure conditions and a decomposition of the laurite layers into Ru und S occurs.

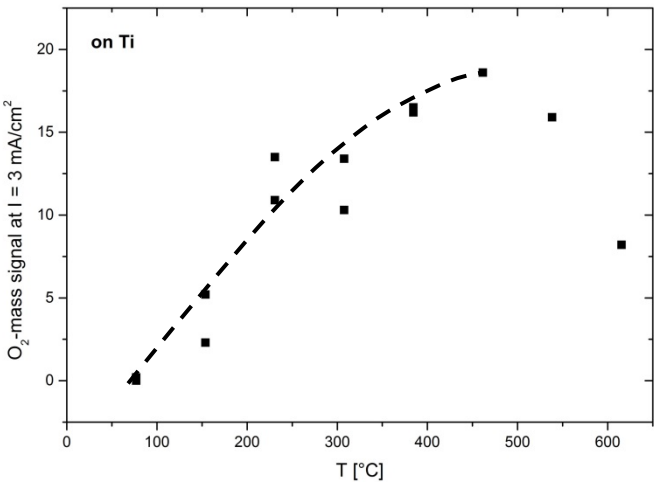

Fig. 8 (c) RuS_2 films deposited on Ti substrates at different deposition temperatures. Highest activity in the oxygen evolution reaction was found with laurite electrodes deposited at 460°C.

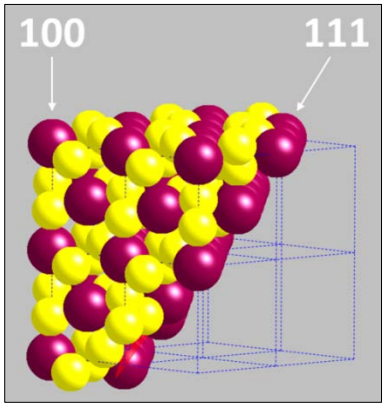

Fig. 9 Eight laurite unit cells partially occupied by Ru and S atoms. A (111) face is either terminated by Ru or by a complex layer of S atoms. In contrast, the (100) surface is smooth and characterized by the mixed presence of Ru atoms and S_2 dumbbells.

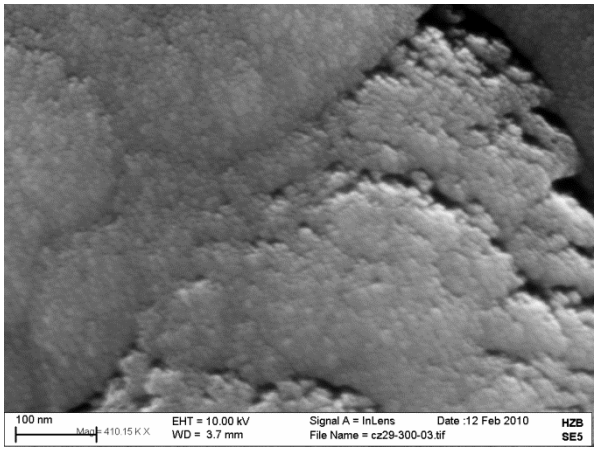

Fig. 10 (a) Scanning electron micrograph of a laurite layer deposited at 240°C.

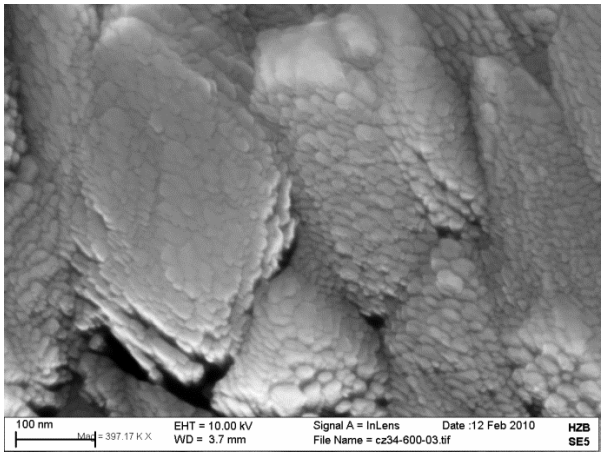

Fig. 10 (b) Scanning electron micrograph of a laurite layer deposited at 460°C.